Journal of Engg. Research **Vol. 4 No. (3) September 2016** pp. 95-113

تنفيذ الاختبارات المعملية للسيارات الكهربائية المزوده بمحركات التيار المستمر المدعومة بخلايا الوقود الهيدروجينية ذات الغشاء البروتيني

عبدالرحمن العثمان، نبيل أحمد، مشعل الشريدة، خالد النجار وبدر العجمي
قسم الهندسة الكهربائية، كلية للدراسات التكنولوجية، الكويت

الخلاصة

المركبات التي تعمل بخلايا الوقود هي أكثر كفاءة نسبيا بالمقارنة مع السيارات التقليدية من حيث تحويل الطاقة ولا تشكل أي خطر على المناخ لأنها لا تسبب أي انبعاثات للغازات الخطرة. في هذا البحث تم استخدام معالج الإشارات الرقمية dSPACE DSP للتحكم في سرعة محرك تيار مستمر يمثل محرك سيارة كهربائية يغذى من خلية وقود ذات غشاء بروتوني من خلال مقطع تيار مستمر رافع للجهد. حيث يجعل استخدام معالج الإشارات الرقمية عملية السيطرة تتم ببساطة ومرونة ولا تحتاج الى نموذج رياضي معقد للمركبة. كما تم دراسة متانة النظام واستجابته العابرة في ظل التغيرات المفاجئة للحمل للتحكم وتثبيت سرعة السيارة. وشملت الدراسة موجات كل من التغير في السرعة والجهد والتيار. وأثبتت النتائج التجريبية أن فاعلية ودقة النظام المقترح.

Experimental implementation of PEM fuel cell powered DC motor for vehicle applications

A. K. Al-Othman*, Nabil A. Ahmed, M. E. AlSharidah, K. M. El-Naggar and Bader N. Alajmi

Department of Electrical Engineering, College of Technological Studies, Alrawda, 73452, P.O. Box 33198, Kuwait

**Corresponding author: ak.alothman@paaet.edu.kw*

ABSTRACT

Fuel cell based vehicles, when compared to conventional vehicles, are relatively more efficient in terms of energy conversion and do not pose any threat to climate due to no emissions of hazardous gases. An implementation of closed loop speed control of a separately excited DC motor for vehicle applications using dSPACE DSP is proposed in this paper. The DC motor is fed by a proton exchange membrane (PEM) fuel cell through a boost converter. Experimental verification has been carried out using dSPACE DS1103-based digital signal processor. The system robustness and transient response have also been studied under sudden load changes to prove feasibility.

Keywords: Boost converter; electric vehicles; dSPACE; fuel cell.

INTRODUCTION

Fuel cells (FCs) are devices that convert chemical energy directly and continuously into electrical energy. The elements of the reaction are pure hydrogen (fuel), oxidant, and oxygen; whereas water, heat and electricity are the products of the reaction. Principally, FCs are direct single stage energy conversion devices that provide relatively high electrical energy conversion efficiency. FC systems, offer a clean alternative for energy production and are considered one of the most promising technologies to be used in the near future, as power supply sources, in various portable applications (Jia *et al.,* 2009; Ceraolo *et al.,* 2003; Amphlett *et al.,* 1996; Talj *et al.,* 2010; Ahmed, 2008). The FCs have characteristic features, such as high efficiency, zero/low pollutant emissions and fuel flexibility, which makes it an extremely desirable option for future power generation. There are many types of fuel cells; e.g., proton exchange membrane (PEM), solid oxide (SO) and molten carbonate (MC). The PEM fuel cell, in particular, has been widely employed in distributed generators and portable applications, due to its reliability in suppling power during steady state operation (Larminie & Dicks,; 2003; Mazumder *et al.,* 2004; Song-Yul *et al.,* 2008; Vepa 2012, Caisheng & Nehrir, 2007).

Over the past two decades, investigation of PEM fuel cells has risen dramatically (Jeong & Oh, 2002; Jia *et al.,* 2009). Such interest is driven by developments in membrane technology, which eventually improved PEM fuel cell performance. In addition, the use of more efficient catalysts made PEM fuel cells more amenable to operation with methanol through new bimetallic electro catalysts, which in turn led to a major reduction in their cost. PEM fuel cells have been targeted as a likely power plant for hybrid electric vehicles and a viable replacement of internal combustion (IC) engine in alternative energy transportation applications (Uzunoglu & Alam, 2007; Ramos-Paja *et al.,* 2009; Ahmed, 2008; Yoon-Ho & Sang-Sun, 1999).

As of recent, employment of fuel cells to supply electric vehicles is becoming popular and is considered an appealing long-term option to power vehicles (Helmolt & Eberle, 2007). Unlike internal combustion engines, the energy conversion in fuel cell powered vehicles is direct (i.e. no combustion). Such features allow for higher efficiency and practically zero emission (Feroldi *et al.,* 2009). In fact, the efficiency of a hydrogen fuel cell-based vehicle is double the efficiency of a conventional internal combustion gasoline vehicle (Rajashekara, 2000; Jeong & Oh, 2002). Additionally, the fuel cell efficiency is comparatively high at partial loads (Friedman & Moore, 1998). Therefore, fuel cell-based vehicles appear to be promising in the future of main stream vehicle industry, as they are potentially more efficient and have no detrimental effect on the environment (Chan, 2002).

In this paper an application of dSPACE DS1103 to control the speed of a separately exited DC motor fed by (PEM) fuel cell is proposed. The control scheme has been developed using MATLAB/Simulink toolbox. The dSPACE DSP allows for both data acquisition and implementation of control scheme in real time. The instantaneous motor speed is measured and compared to a preset desired reference speed. The error is amplified via proportional-integral (PI) controller in an effort to accommodate any disturbance in the speed, and consequently, a proper PWM triggering signal is generated to control the IGBT switch of the boost converter for voltage regulation, to achieve real time speed control of DC motor.

STEADY STATE MODEL OF FUEL CELL

Polymer electrolyte membrane fuel cell (PEM FC) is a low temperature fuel cell. The PEM FC is composed of two catalyst coated electrodes and electrolytes. The electrodes are made of a porous material called cathode and anode, which are located on the electrolytic layer sides. As the Hydrogen is passed through the anode and catalyst, it gets oxidized and separates into protons and electrons. At the cathode the electrons coming through the external circuit are combined with the protons and the oxygen from the ambient air to produce water and heat according to the following chemical reactions:

At the anode:

$$H_2 \rightarrow 2H^+ + 2e^- \tag{1}$$

At the cathode:

$$2H^+ + \frac{1}{2}O_2 + 2e^- \rightarrow 2H_2O \tag{2}$$

The net reaction:

$$H_2 + \frac{1}{2}O_2 \rightarrow H_2O \tag{3}$$

Open circuit voltage

The energy of the chemical reaction is difficult to define in terms of electrical power and energy. The open circuit voltage is a function of the change in the Gibbs free energy Gf^o of the product water and the Gibbs free energy of the inputs, or reactant gases hydrogen and oxygen. The Gibbs free energy is variable in terms of temperature, pressure and state (liquid or gas). Using the thermodynamics argument and the change in molar Gibbs free energy, the chemical reaction is given by Equation (1); the open circuit voltage (E) at any operating temperature and pressure is given by (Song-Yul *et al.,* 2008):

$$E = \frac{-\Delta Gf^o}{2F} + \frac{RT}{2F}\ln\left(\frac{P_{H_2}.P_{O_2}^{\frac{1}{2}}}{P_{H_2O}}\right) \tag{4}$$

where R is the universal gas constant (8.314JK^{-1}mol^{-1}), T is the temperature in Kelvin, $F = N.e = 96485\,C$ is the Faraday's constant, P_{H_2O}, P_{H_2} and P_{O_2} are the partial pressure of water, hydrogen and oxygen, respectively. Equation (4) provides an open circuit voltage of about 1.2 V for a fuel cell operating below 100ºC. In practice, this value may be less than the value obtained by Equation (4), due to voltage drop. The open circuit voltage may be given as follows:

$$E = 1.229 - 0.85\times10^{-3}(T - 298.15) + 4.308\times10^{-3}T\ln(P_{H2}P_{O2}^{\frac{1}{2}}) \tag{5}$$

The output voltage of the PEM FC does not match the theoretical maximum voltage, i.e. open circuit voltage. This is due to losses within the PEM FC. Taking into account such losses, the net output voltage of the PEM FC as described by Song-Yul *et al.,* 2008) and Caisheng & Nehrir, 2007 and Ahmed, 2008 is:

$$V = E - V_{act} - V_{ohm} - V_{trans} \tag{6}$$

where V_{act} is the activation voltage drop across the anode and cathode, V_{ohm} is the Ohmic voltage drop, and V_{trans} is the concentration of the reactant gases voltage drop. A detailed PEM FC model is presented by Song-Yul *et al.,* 2008 and Ahmed, 2008.

Activation voltage drop

Activation voltage drop depends on the rates of chemical reaction on the surface of the electrodes. Part of the open circuit voltage is consumed to drive the chemical reaction within the PEM FC. The activation voltage drop increases proportionally to the increase in cell current. An extremely fast reaction of the PEM FC can be obtained, if FC operates at high temperatures. At low temperatures, the voltage drop PEM FC is expected to be relatively substantial and highly nonlinear, which can be characterized by Equation (7):

$$V_{act} = -[\xi_1 + \xi_2 T + \xi_3 T \ln(i) + \xi_4 T \ln(C_{O2})] \tag{7}$$

where CO_2 is the dissolved Oxygen concentration at the cathode/membrane interface. Equation (7) corresponds to an early empirical equation by Tafel (Uzunoglu & Alam, 2007).

Internal current and fuel crossover

The membrane of FC has been selected for its low ion conducting properties; a few electrons take their paths across the membrane, causing internal currents. Also, some fuel will diffuse from the anode through the electrolyte to the cathode, where it will react directly with the oxygen producing no current from the cell. This small amount of wasted fuel that passes through the electrolyte is known as fuel crossover. The effect of internal currents and fuel crossover are equivalent and the fuel cell crossover is more important. This effect is not very important, but in low temperature operation as in PEM FC, it can cause a remarkable voltage drop (Ahmed, 2008; Larminie & Dicks, 2003). Due to the internal current density, the cell current is not zero even at open circuit. This voltage drop is not easy to measure, but it can be represented by a constant current i_n added to the cell current as follows:

$$V_{cell} = E - A \ln\left(\frac{i + i_n}{i_o}\right) \tag{8}$$

Where A is the Tafel equation constant, i_o is the no-load current density (i_o is small and generate negative logarithm) and i is the cell current density. A and i_o are electrode and cell conditions dependents.

Ohmic losses

The electrical resistance of the electrodes causes part of the Ohmic voltage losses. In addition, other losses can be contributed from the resistance due to the flow of ions in the electrolyte and the cell interconnectors (Ahmed, 2008; Larminie & Dicks, 2003). The Ohmic voltage drop is found to be linearly proportional to the cell current and given by:

$$V_{ohm} = -i[R_M + R_C] \tag{9}$$

where R_m and R_c are the membrane and connector resistors respectively.

Concentration or mass transportation voltage losses

During PEM FC operation, reduction in oxygen concentration at the cathode naturally will cause mass transportation voltage drop. The rate at which the current being drawn from the PEM FC directly affects the oxygen concentration. At the cathode, the change in oxygen concentration leads to a drop in oxygen pressure. Also, the increase of current drawn from the PEM FC will result in similar drop in the hydrogen pressure at the anode. This mass transport voltage or concentration loss becomes significant at higher currents when the hydrogen and oxygen are used at higher rates (Ahmed, 2008, Larminie & Dicks, 2003). Equation (7) displays the voltage drop losses due to concentration or mass transport losses.

$$V_{trans} = -B\ln\left(1 - \frac{i}{i_m}\right) \tag{10}$$

where i_m is limiting current density, and represents the maximum current produced when the surface concentration of reactant is reduced to zero at the reaction site. However, in reality, the assumption of a completely mass-transfer limiting case is rarely valid (Mench *et al.,* 2001)**.**

Numbers of individual cells are stacked in a series to form a fuel cell power module to obtain the desired value of terminal voltage and electrical power. Increasing the number of cells in a stack increases the output voltage (Ahmed, 2008; Larminie & Dicks, 2003), while increasing the surface area of the individual cells increases the output current. Table 1 indicates the typical parameters of Ballard Nexa 310-0027 power module of PEMFC used in this study.

Table 1. Single PEMFC model parameters

Item	Symbol	Value
Reversible open circuit voltage	E	1.2 [V]
Tafel equation constant	A	0.03 [V]
Exchange current density	i_o	0.08 [mAcm^{-2}]
Internal and crossover current density	i_n	3.26 [mAcm^{-2}]
Area specific resistance	n	2.45e^{-4} [kΩcm^{-1}]
Constants of concentration or mass transfer losses	m	2.11e^{-5} [V]
Constants of concentration or mass transfer losses	n	7.8e^{-3} [cm^{-2}mA^{-1}]

Typically, the V-I characteristics of a FC posses three main regions, a very steep or non-linear rapid initial fall in the cell voltage from the open circuit voltage at low currents due to the activation and internal current losses. Then, there is a linear drop due to Ohmic losses. After that, and at higher current density, there is a rapid voltage drop due to mass transport and concentration losses. It is depicted that as the current density increases, the output voltage decreases and it is worthy to note that there is a limiting current at which the fuel cell should operate.

CIRCUITS DESCRIPTIONS AND PRINCIPLE OF OPERATION

Typically, an electric vehicle is a vehicle supplied by an electrical source. The power bus is a dc link between source and load. FCs that produce dc voltage outputs can be connected to electric power networks through power conditioning units such as DC-DC and DC-AC inverters. Various topologies of power converter may be utilized as an interface between the FC and the load (Thounthong *et al.,* 2009).

The schematic diagram and the system configuration of a FC powered boost DC-DC converter fed separately exited DC motor is shown in Figure 1. When the chopper switch is turned on, diode D is reverse biased and the output stage is isolated from the input. The FC supplies energy to the boost inductor and the boost inductor current increases linearly and energy is stored in the inductor. When the chopper switch is turned off, the energy stored in the boost inductor is transferred to the motor through the diode and the boost inductor current decreases linearly. The output stage receives energy from FC and the boost inductor. Therefore the output voltage is boosted. The output voltage is maintained constant by connecting a large capacitor across the motor terminal and it will be continuous and its value will be the average value. The voltage across the motor can be controlled / adjusted by varying the converter duty cycle D, and the minimum motor voltage is the fuel cell voltage V_s when D equals zero.

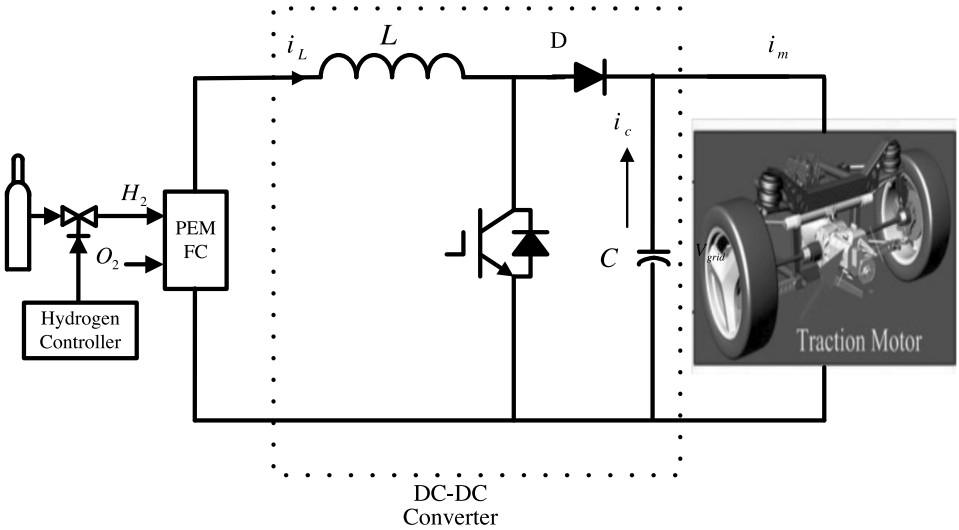

Fig. 1. System configuration of boost converter fed electric vehicle.

The armature voltage equation of a separately exited DC motor is given by:

$$v_m = R_a i_m + L_a \frac{di_m}{dt} + k_m \omega_m \tag{11}$$

and the electromagnetic torque equation can be written as

$$T_e = T_L + J \frac{d\omega_m}{dt} + B\omega_m \tag{12}$$

where k_m is the motor constant and given by

$$k_m = k_v i_f \tag{13}$$

The operation principle during one switching period is divided into two switching modes: charging and discharging modes. Figure 2 illustrates the steady-state voltage and current waveforms during one complete period.

Charging mode (Mode1)

This mode is valid for the time $0 \le t < DT_s$, T_s is the switching period, the switch S_w is closed and the diode D becomes reverse biased so the FC voltage V_s appears across the boost inductor. The energy is transferred from the FC V_s to the boost inductor. The current i_L increases linearly through the input side, resulting in charging the inductor. During this mode, the capacitor C and the motor terminals are disconnected from the FC. Therefore, the capacitor begins to discharge through the armature winding and the

motor current continues to flow through the capacitor C. The system stays in this mode until the boost switch is turned off. The following performance equations in this mode can be found as follows:

The boost inductor current for mode 1 is:

$$v_s = L\frac{di_L}{dt} \tag{14}$$

$$i_s = i_L \tag{15}$$

The motor current for mode 1 can be found from

$$i_m = i_c \tag{16}$$

$$i_c = C\frac{dv_m}{dt} \tag{17}$$

Discharging mode (Mode 2)

During the off time $DT_s < t < T_s$ of the boost switch S_w, the diode D will be forward biased and the inductor current decreases through the input and output sides. The output stage receives energy from the input FC as well as from the boost inductor. Hence, output voltage becomes greater than the FC voltage.

The boost inductor current for mode 2 can be found from

$$L\frac{di_L}{dt} = v_s - v_m \tag{18}$$

$$i_s = i_L \tag{19}$$

$$i_L = -i_c + i_m \tag{20}$$

$$i_c = C\frac{dv_m}{dt} \tag{21}$$

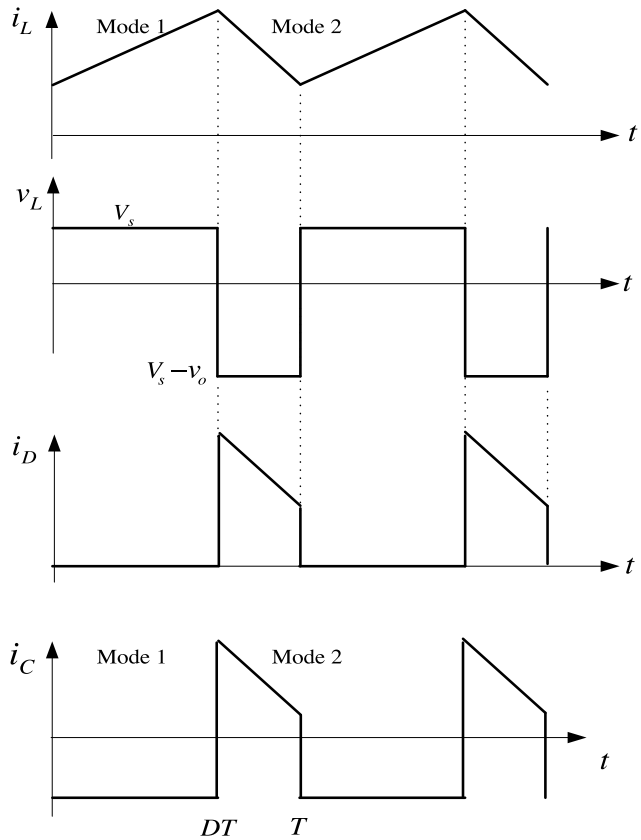

Fig. 2. Current and voltage waveform during one switching period.

Using open loop speed control, the motor can be operated at any intermediate speed by changing the applied voltage or armature current (chopper output voltage). In this case the speed cannot be precisely adjusted due to load variations on the motor shaft. Therefore, a closed loop control is essential for motor applications in electric vehicles, where constant speed is required in which the motor measured speed is fed back to the speed controller. The block diagram of a closed-loop boost converter fed DC motor is shown in Figure 3. A speed sensor is connected to the shaft; the measured speed of the sensor ω is fed back and compared with the reference speed ω^* to form the speed error ω_e. The difference speed error is applied to the speed controller to generate a control voltage V_c which adjusts the boost converter duty cycle to produce the desired terminal voltage V_a. This terminal voltage controls the vehicle speed and thus it can be maintained for any variations in the load torque. If the vehicle speed decreases from its desired value due to the application of additional load torque, the speed error V_e at the output of the comparator increases. The speed controller acts accordingly with an increased control signal V_c to increase the duty cycle of the boost converter and thus

the output terminal voltage V_a will increase. This increased armature voltage develops more torque to compensate the effect of applied load torque and to restore the motor speed to its original value. In contrast, if the speed of the vehicle is increased due to load reduction, the same operation in the reverse way will be performed. When the produced electromagnetic torque matches the load torque, then the vehicle speed will remain constant at its reference speed.

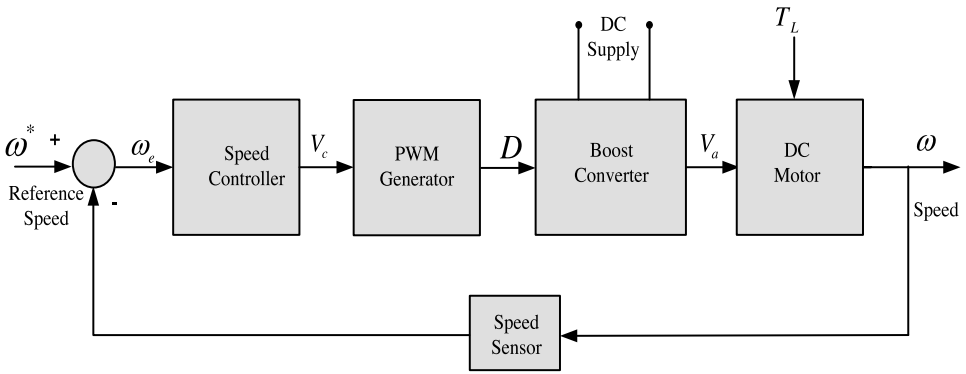

Fig. 3. Block diagram of closed-loop boost converter fed DC motor.

Controller design parameters

Various modern control techniques, such as model predictive control, adaptive control, variable structure control and intelligent control, have been intensively studied for controlling the nonlinear components. However, these control techniques have few real applications probably due to their complicated structures and the lack of their stability. Therefore, in this paper conventional proportional-integral (PI) speed controller is used because of its simple structure, less steady sate error and smooth response. Generally, the speed error, which is the difference of reference speed (ω^*) and actual speed (ω), is given as input to the PI controller. The controller processes the speed error and gives the control voltage V_c which adjusts the boost converter duty cycle and produces the desired armature voltage V_a.

$$V_c = k_p(\omega^* - \omega) + k_i \int (\omega^* - \omega))\, dt \tag{22}$$

where K_p and K_i are the PI speed control parameters.

The general block diagram of the PI controller is shown in Figure 4.

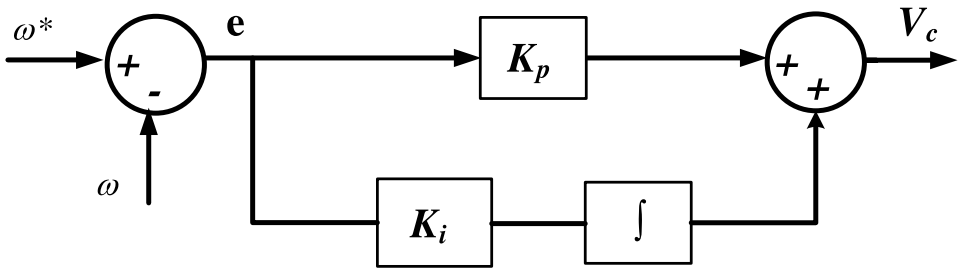

Fig. 4. Block diagram of PI controller.

Unfortunately, tuning the parameters of the PI controller properly is tedious due to the nonlinearity and the high complexity of the system (Qiao *et al.,* 2006). Several methods have been introduced for tuning PI controllers, mostly based on heuristic techniques; to combat such difficulty i.e. genetic algorithms (GA), particle swarm optimization method (PSO) and fuzzy logic (Gozde & Taplamacioglu, 2011; Feng *et al.,* 2003; Mitsukura *et al.,* 1999; Kecskés & Odry, 2014; Kim *et al.,* 2008; Allaoua *et al.,* 2009; Popov *et al.,* 2005).

In this study, the speed controller parameters (K_p, K_i) were chosen after an in depth evaluation and a number of trial and evaluation attempts. A value of $K_p = 0.01$ and $K_i = 0.00082$ was selected, which allows fast tracking of the command speed with relatively minimal ripple.

This part of the controller is completely implemented in the DS1103 dSPACE digital signal processing control board.

DSPACE DESCRIPTION

The dSPACE system is a commonly used tool as a controlling platform and is particularly utilized in automation systems, car manufacturing industries and many other industrial applications that involve on-line monitoring and control. The dSPACE is a digital signal processing system that acts as a tie between control models, which are built in MATLAB/SIMULINK, and the hardware circuitry desired to be controlled. To carry out the linkage task, software support is provided to facilitate input/output ports and peripherals through real time interface (RTI) library to read in and write out measured variables. Such I/O peripherals are A/D conversion, 16 parallel A/D converters supporting conversion mode, D/A conversion, 4 parallel D/A converters, digital I/O unit, 40 digital input channels and 40 digital output channels that can be used for (bit I/O, PWM, signal generation (PWM), square-wave signal generation, PWM signal measurement, frequency measurement and incremental encoder interface. The dSPACE DS1103 controller board contains the core processor PowerPC603 with a clock speed of 250 MHz, a 64-bit floating-point processor, and a 16-bit DSP-Texas

Instruments TMS320F240 microcontroller. This controller is very appealing for modeling and prototyping due to its cost-sensitive rapid control prototyping feature. It is particularly appropriate for the development of high-speed multivariable digital controllers and real-time simulations in various fields (DS1104, 2008).

When a given control scheme is designed and built in Simulink (including the required interface blocks for input and output ports), C-code is generated by means of real time workshop (RTW) functions. The C-code is compiled, linked and loaded in memory to be executed, thereby performing the required controlling task. The dSPACE platform is accompanied by a software package called ControlDesk Next Generation. This package supports some basic features of the automation to allow for comprehensive real time control and monitoring of the control routine. The control desk environment provides multiple purposes. It provides the interface for downloading controller models on the DSP and provides the ability to interface with the entire system; so, inputs, such as the desired motor speed, can be altered. Output data can be monitored on the PC display in real-time and several other measuring instruments to measure and display data from the experimental setup. This allows for checking and validation of the system operation in real-time by displaying the variables, adjusting the system parameters and saving results.

EXPERIMENTAL VALIDATION AND DISCUSSIONS

To verify the principle of operation and the accuracy of the results of the proposed system, a prototype is built in the laboratory and checked for different case studies. The system configuration for the experimental setup is divided into two parts: the dSPACE DS1103-based digital signal processor and the power circuit. The dSPACE-based control board enables software flexibility and allows implementation of the proposed control. The power circuit prototype rating of 1.0 kW (200V, 5A) has been implemented using POWEREX CM150DY-12H IGBT as the boost switch, CS241210 fast recovery diode and DC motor rated 1.0 kW, 200V, 5 A, 1500 rpm coupled to a DC generator as an electric load. The parameters of the hardware components of the circuit used for experiments and simulation are presented in Table 2. The switching frequency used is 10 kHz. Ballard Nexa 310-0027 PEM FC power module is used in this study as a power source. The experimental setup is shown in Figure 5.

Table 2. Simulation constants and circuit parameters

Parameter	Symbol	Value
Fuel cell voltage	V_{fc}	30.0[V]
Vehicle rated voltage	V_m	150.0[V]
Switching frequency	f_s	5.0 [kHz]
Armature resistance	R_a	2.95 [Ω]
Armature inductor	L_a	0.095[H]
Motor constant	K_m	1.53[$V/(rad/s)$]
Moment of inertia	J	0.078[$kg.m^2$]
Boost Inductor	L	33.0[mH]
Capacitor	C	3300[μF]
PI Controller parameters	K_i	0.00082
	K_p	0.01

Figure 4 illustrates the power stage and the fuel cell of the experimental setup. The voltage and current signals have been measured by LV 55-P and LA-55-P voltage and current transducers and the speed was measured by TECNEL (60V/1000 rpm) tacho-generator. The tacho-generator voltage is not perfectly DC and has some voltage ripple. So, a filter is used to smooth the measured speed signal. VLA536-01R IGBT driver circuitry is used as an interface between the dSPACE and the IGBT boost switch. It must be noted that due to limitation of the available measuring oscilloscope, as it cannot accommodate the required bandwidth, all measured data are monitored in real time and saved to the PC through Control Desk Next Generation ver. 5 accompanied with dSPACE platform for analysis interpretation and plotting.

To assess both validity and viability of the proposed system, a series of experimental tests were performed. Discussion of experimental results is presented in the following.

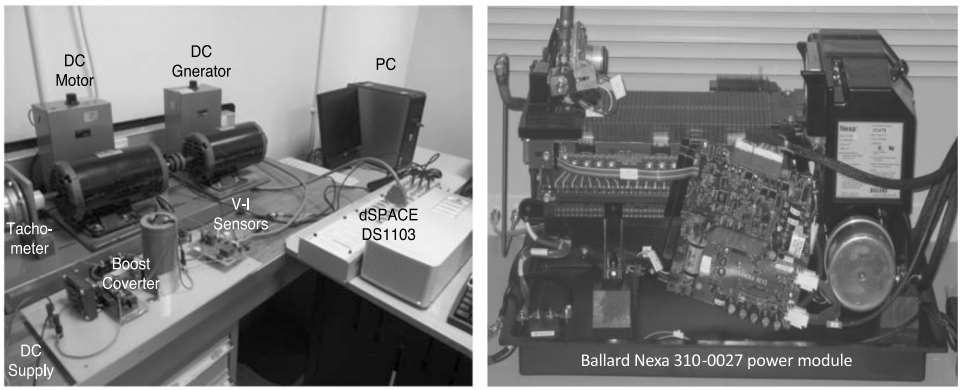

Fig. 5. Test bench of the fuel cell (Ballard Nexa 310-0027 power module) fed DC motor

In order to evaluate the transient response and tracking performance of the proposed system, a speed reference pattern was carried out sequentially with speed profile of 820, 1100, 1380, 1100 and 920 rpm respectively. Each command lasts 20 seconds and after each elapsed period, the speed reference is changed. The transient response of the variable states (vehicle side) is presented in Figure 6. Those variable states are vehicle speed, duty cycle, applied voltage and drawn current by vehicle, respectively. The results show that the system is capable of tracking the reference speed very well. The corresponding variables at the input side of fuel cell voltage and current are shown in Figure 7.

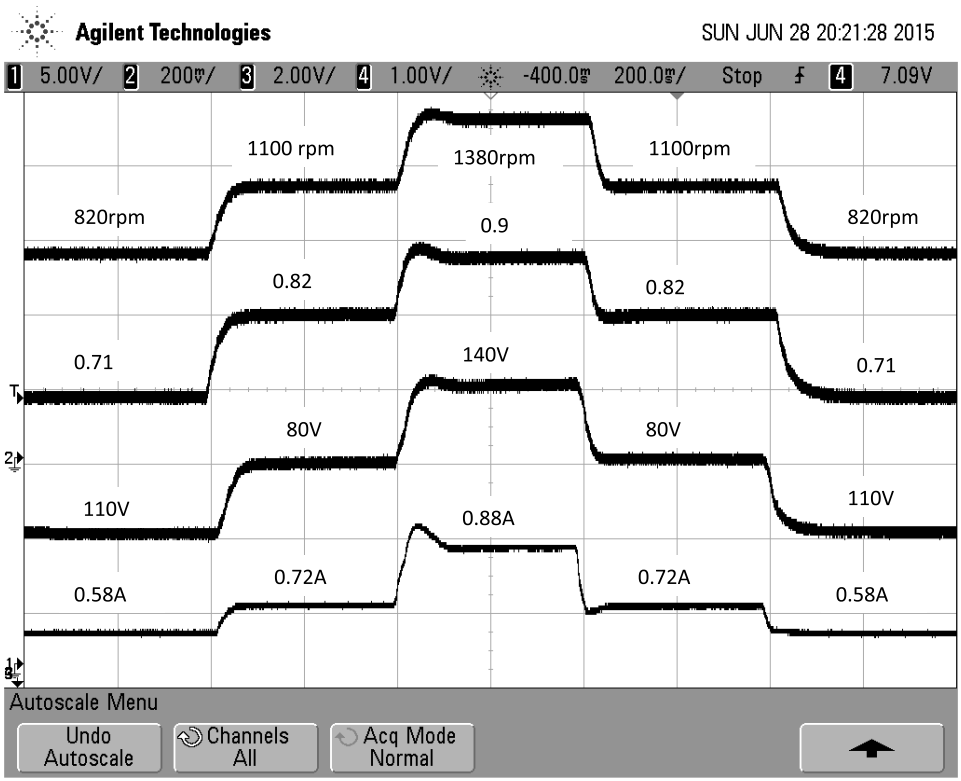

Fig. 6. Performance of vehicle control, vehicle speed, duty cycle, vehicle voltage and current

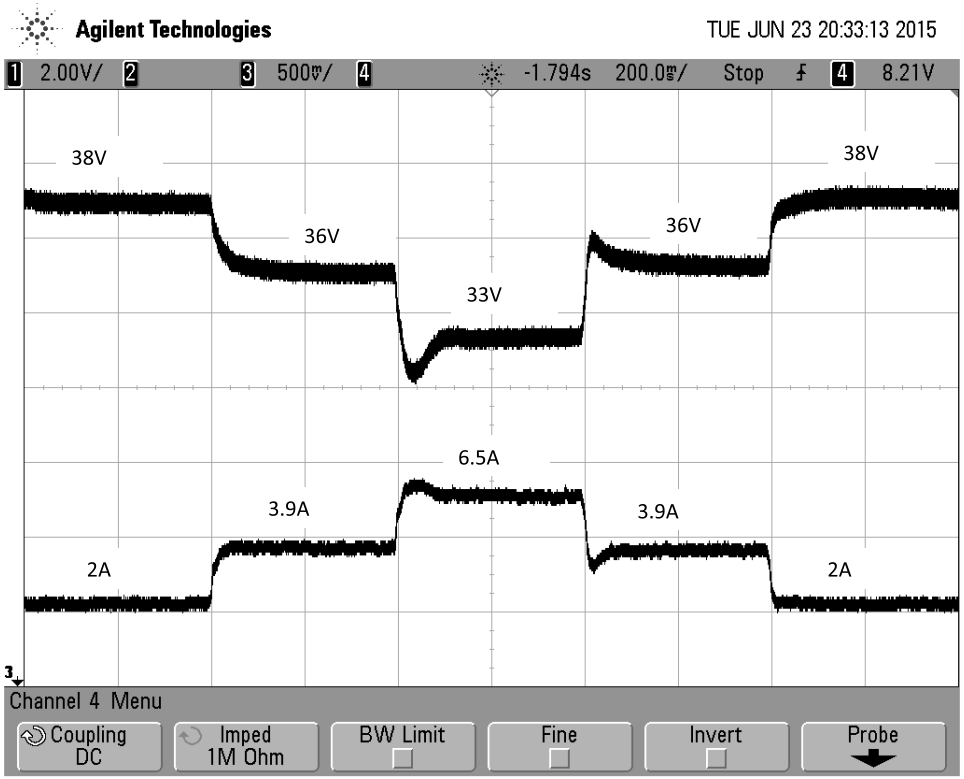

Fig. 7. Fuel cell voltage (upper trace) and current (lower trace).

To validate the robustness of the proposed controller, the system is examined under load disturbance with constant reference speed command. The transient response of the proposed system due to sudden load changes at the vehicle is shown in Figure 8. While the vehicle is running at load, the load is suddenly removed at time of 30s then applied again at time 60s. Figure 78 (first trace) illustrates the experimental variation of the vehicle speed. It is clear that the actual speed of the vehicle tracks the reference speed command. At time of 30s the speed started to increase due to the load removal; the speed controller responded with a decreased control signal. This resulted in a decrease in the duty cycle. Consequently, the vehicle applied voltage is adjusted to the value required to retain the vehicle speed to its reference value as shown in Figure 8 (second trace). At time of 60s, the speed tended to decrease due to the load addition, but the speed controller responded by increasing the duty cycle. Therefore, higher armature voltage was applied, keeping constant speed operation. The results shown in Figure 8 (first trace) provide excellent speed control for sudden load disturbance. Figure 8 (third and fourth traces) depicts the relevant voltage and current waveforms for the same step change in the load torque, while figure 9 depicts the relevant fuel cell voltage and current variations.

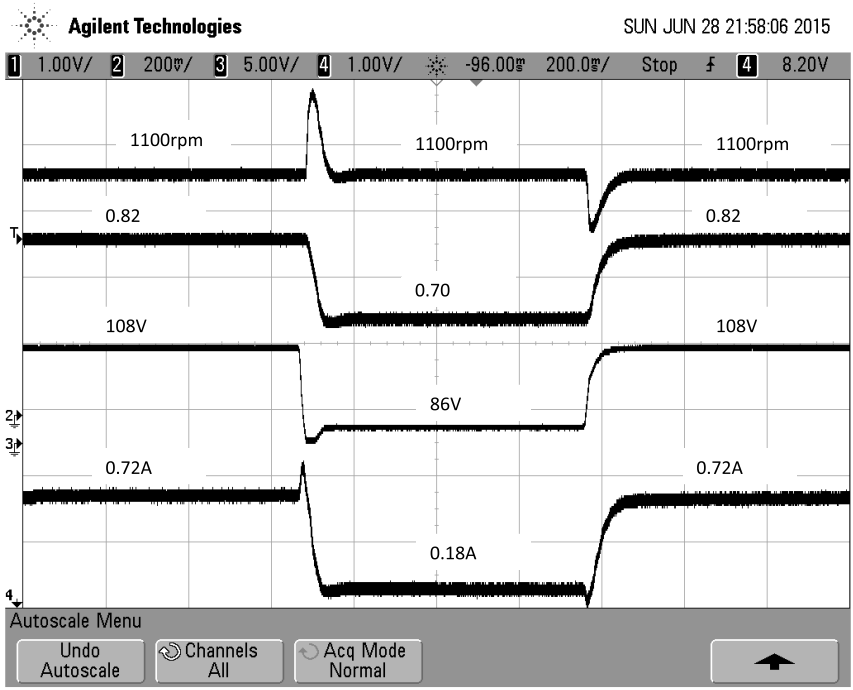

Fig. 8. Experimental response at negative and positive load torque disturbances, motor speed, duty cycle, motor voltage, motor current.

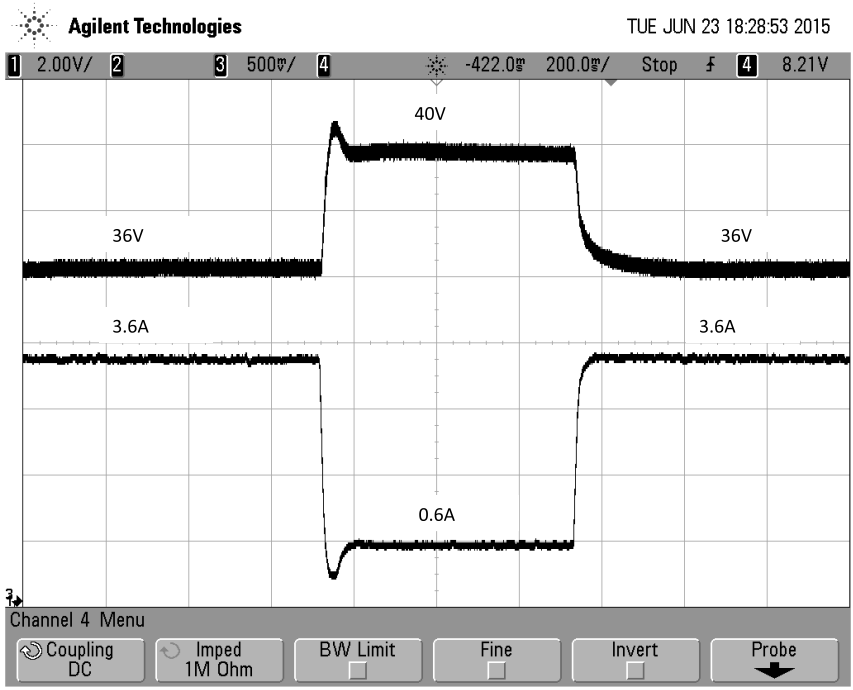

Fig. 9. Fuel cell voltage and current at negative and positive load torque disturbances.

CONCLUSIONS

A practical implementation of dSPACE control board for speed control of a PEM fuel cell fed electric vehicle is presented in this paper. The dSPACE DS1103 controller platform is employed as an interface between MATLAB/Simulink and hardware, in order to execute the on-line vehicle control scheme and manipulate various variables and parameters such as vehicle speed, voltage and current. The use of dSPACE DSP makes the control process simpler, flexible and does not need a complicated mathematical model of the electric vehicle. That in turn, leads to less computational time and a faster control response. The control scheme was implemented experimentally under different reference speed commands and sudden load changes. The experimental outcomes proved that the proposed setup is efficient, accurate and above all environmentally suitable due to a reduced amount of carbon dioxide (CO2) emission for a given power output.

ACKNOWLEDGMENT

This work is supported and funded by The Public Authority for Applied Education and Training, Research Project No(TS-15-03) dSPACE Control of PEM Fuel Cell for Speed Control of DC Motor.

REFERENCE

Ahmed, N.A. 2008. Computational modelling and polarization characteristics of proton-exchange membrane fuel cell with evaluation of the interface systems. Journal of European Power Electronic, 18: 32-41.

Allaoua, B., Gasbaoui, B. & Mebarki, B. 2009. Setting up PID DC motor speed control alteration parameters using particle swarm optimization strategy. Leonardo Electron J Pract Technol, 14:19–32.

Amphlett, J.C., Mann, R.F., Peppley, B.A., Roberge, P.R. & Rodrigues, A. 1996. A model predicting transient responses of proton exchange membrane fuel cells. Journal of Power Sources, 61:183-188.

Caisheng, W. & Nehrir, M.H. 2007. Fuel cells and load transients. Power and Energy Magazine, IEEE, 5:58-63.

Chan, C.C. 2002. The state of the art of electric and hybrid vehicles. Proceedings of the IEEE, 90:247-275.

DS1104 2008. dSPACE DS1104, Hardware installation and configuration and controldesk experiment guide, Paderborn, Germany.

Feng, X., Donghai, L. & Yali, X. 2003. Comparing and optimum seeking of PID tuning methods based on ITAE index. Proceedings of the CSEE, 23.

Feroldi, D., Serra, M. & Riera, J. 2009. Energy management strategies based on efficiency map for fuel cell hybrid vehicles. Journal of Power Sources, 190:387-401.

Friedman, D.J. & Moore, R.M. 1998. PEM fuel cell system optimization. Proceedings of the 2nd International Symposium on Proton Conducting Membrane Fuel Cells II. Electrochemical Society. Pennington, NJ, U.S.A.

Gozde, H. & Taplamacioglu, M.C. 2011. Automatic generation control application with craziness based particle swarm optimization in a thermal power system. Int J Electr Power Energy Syst, 33:8-16.

Helmolt, R. & Eberle, U. 2007. Power management and design optimization of fuel cell/battery hybrid

vehicles. Journal of Power Sources, 165:833-843.

Jeong, K. & Oh, B. 2002. Fuel economy and life-cycle cost analysis of a fuel cell hybrid vehicle. Journal of Power Sources, 105:58-65.

Jia, J., Li, Q., Wang, Y., Cham, Y.T. & Han, M. 2009. Modeling and dynamic characteristic simulation of proton exchange membrane fuel cell. IEEE Trans. Control Syst. Technol, 24:283-291.

Kecskés, I. & Odry, P. 2014. Optimization of PI and fuzzy-PI controllers on simulation model of szabad(ka)-II walking robot. International Journal of Advanced Robotic Systems, 11:1-13.

Kim, T.H., Maruta, I. & Sugie, T. 2008. Robust PID controller tuning based on the constrained particle swarm optimization. Automatica, 44:1104 –1110.

Larminie, J. & Dicks, A. May 2003. Fuel Cell Systems, Explained, John Wiley & Sons Inc.

Ceraolo, M., Miulli, C. & Pozio, A. 2003. Modelling static and dynamic behaviour of proton exchange membrane fuel cells on the basis of electro-chemical description. Journal of Power Sources, 113:131-144.

Mazumder, S.K., Acharya, K., Haynes, C.L., Williams, R., Jr., Von Spakovsky, M.R., Nelson, D.J., Rancruel, D.F., Hartvigsen, J. & Gemmen, R.S. 2004. Solid-oxide-fuel-cell performance and durability: resolution of the effects of power-conditioning systems and application loads. Power Electronics, IEEE Transactions on, 19:1263-1278.

Mench, M.M., Wang, C.Y. & Thynell, S. 2001. An introduction to fuel cells and related transport phenomena. International Journal of Transport Phenomena, 3:151-176.

Mitsukura, Y., Yamamoto, T. & Kaneda, M. 1999. A design of selftuning PID controllers using a genetic algorithm. Proc. Amer. Contr. Conf. San Diego, CA.

Popov, A., Farag, A. & Werner, H. 2005. Tuning of a PID controller Using a Multi-objective Optimization Technique Applied to A Neutralization Plant. 44th IEEE Conference on Decision and Control and the European Control Conference 2005.

Qiao, W., Venayagamoorthy, G. & Harley, R. 2006. Design of optimal PI controllers for doubly fed induction generators driven by wind turbines using particle swarm optimization. IEEE 2006 international joint conference on neural networks (IJCNN '06). Georgia Institute of Technology, Atlanta, U.S.A.

Rajashekara, K. 2000. Propulsion system strategies for fuel cell vehicles. Fuel Cell Technology for Vehicles, 1:179-187.

Ramos-Paja, C.A., Bordons, C., Romero, A., Giral, R. & Martinez-Salamero, L. 2009. Minimum fuel consumption strategy for PEM fuel cells. Industrial Electronics, IEEE Transactions on, 56:685-696.

Song-Yul, C., Jong-Woo, A., Jung-Gi, L. & Soo-Hyun, B. 2008. Dynamic simulator for a PEM fuel cell system with a PWM DC/DC converter. Energy Conversion, IEEE Transactions on, 23:669-680.

Talj, R.J., Hissel, D., Ortega, R., Becherif, M. & Hilairet, M. 2010. Experimental validation of a PEM fuel-cell reduced-order model and a moto-compressor higher order sliding-mode control. Industrial Electronics, IEEE Transactions on, 57:1906-1913.

Thounthong, P., Raël, S. & Davat, B. 2009. Energy management of fuel cell/battery/supercapacitor hybrid power source for vehicle applications. Journal of Power Sources, 193:376-385.

Uzunoglu, M. & Alam, M.S. 2007. Dynamic modeling, design and simulation of a PEM fuel cell/ultra-capacitor hybrid system for vehicular applications. Energy Conversion and Management, 48:1544-1553.

Vepa, R. 2012. Adaptive state estimation of a PEM fuel cell. Energy Conversion, IEEE Transactions on, 27:457-467.

Yoon-Ho, K. & Sang-Sun, K. 1999. An electrical modeling and fuzzy logic control of a fuel cell generation system. Energy Conversion, IEEE Transactions on, 14:239-244.

Submitted: 6/07/2015

Revised: 09/07/2015

Accepted: 09/02/2016